arXiv:cond-mat/0007450v1 [cond-mat.str-el] 27 Jul 2000

Hybrid Monte Carlo algorithm for the Double Exchange Model

J. L. Alonso[1], L. A. Fernández[2], F. Guinea[3],
V. Laliena[1] and V. Martín-Mayor[4]

[1] Dep. de Física Teórica, Facultad de Ciencias, Univ. de Zaragoza, 50009 Zaragoza, Spain.

[2] Dep. de Física Teórica, Facultad de CC. Físicas, Univ. Complutense de Madrid, 28040 Madrid, Spain.

[3] Instituto de Ciencia de Materiales (CSIC). Cantoblanco, 28049 Madrid. Spain.

[4] Dip. di Fisica, Univ. di Roma "La Sapienza", 00185 Roma and INFN sezione di Roma, Italy.

March 21, 2022

Abstract

The Hybrid Monte Carlo algorithm is adapted to the simulation of a system of classical degrees of freedom coupled to non self-interacting lattices fermions. The diagonalization of the Hamiltonian matrix is avoided by introducing a path-integral formulation of the problem, in $d+1$ Euclidean space-time. A perfect action formulation allows to work on the continuum euclidean time, without need for a Trotter-Suzuki extrapolation. To demonstrate the feasibility of the method we study the Double Exchange Model in three dimensions. The complexity of the algorithm grows only as the system volume, allowing to simulate in lattices as large as 16^3 on a personal computer. We conclude that the second order paramagnetic-ferromagnetic phase transition of Double Exchange Materials close to half-filling belongs to the Universality Class of the three-dimensional classical Heisenberg model.

05.10.Ln, 75.10.-b, 75.30.Et

1 Introduction

Most of the models so far proposed to study the Colossal Magnetoresistance manganites (CMR) [1], share an extremely simplifying feature: an assembly of non self-interacting lattice fermion is coupled to an extensive number of classical continuous degrees of freedom (the localized core spins of the Kondo model and of the Double Exchange Model [2], and/or the Jahn-Teller lattice distortion fields [3]). Other physical context where this simplifying feature appear are the pyrochlores or doubles perovskites.

The non self-interacting nature of the electrons in these models makes it possible to explicitly perform the trace in Fock space, in terms of the single-particle eigenstates. This yields a positive Boltzmann weight for the continuous classical degrees of freedom, that for the sake of brevity we will call spins in what follows (although they could be a lattice distortion field!). In principle, the resulting problem could be simulated by means of a Metropolis algorithm. However, the update of a single spin requires a diagonalization of the single-particle Hamiltonian matrix, which has a computational cost proportional to the square of the lattice volume (if the most sophisticated available algorithm is used). This implies that the time needed to update all the spins on the lattice scales at best with the cube of the lattice size. This problem has prevented the study of systems with more than (say) two-hundred spins (a 6^3 lattice) in the simplest of the above quoted models, the Double Exchange model (DEM), although most simulations [4, 5] are done with a hundred or less spins. This is certainly not enough for an accurate study of phase-transitions where most of the interesting physics occurs.

In this paper, we reformulate the problem in the path-integral formalism, obtaining an exact representation on $d+1$ dimensions for the fermions and d dimensions for the (classical) spins. In this representation a positive Boltzmann weight is obtained, and the update of the spins can be done by means of the Hybrid Monte Carlo (HMC) algorithm [6]. For the DEM, the computational cost of a full-lattice updating is empirically found to grow as the lattice volume (although a worst-case estimate would have yielded a square-volume growing). In addition, the autocorrelation time for HMC is proportional to the correlation

length while with the Metropolis algorithm in the Hamiltonian formalism it grows like the correlation length squared. We will show that a standard simulation on a 4^3 lattice yields fully compatible results with our HMC algorithm, but the latter allows to simulate a 16^3 lattice on a personal computer. In this way we are able to obtain meaningful results for the phase diagram of the DEM model. Some attention will be paid to the largeness of the finite-size corrections on the small lattices. We will also show that in the absence of superexchange coupling between the spins (whose numerical treatment is straightforward), the Double Exchange Model near half-filling presents a second order phase transition between the paramagnetic (PM) and the ferromagnetic (FM) phase, that belongs to the Universality Class of the three-dimensional Heisenberg model. Work is in progress for the study of the phase-diagram of the DEM complemented with a first-neighbors antiferromagnetic superexchange interaction. The final goal is to confirm that the antiferromagnetic coupling is able to turn this PM-FM phase transition from second to first order as predicted by Mean-Field [7]. The phenomenological importance of reliably finding PM-FM first-order transitions between phases of very similar electronic densities cannot be overemphasized [8].

The structure of the paper is as follows. In the next section we describe the DEM, introducing our notational conventions and deriving it from the Kondo lattice model. This somehow academic exercise will allow to introduce in a natural way a mathematically equivalent formulation of the DEM in terms of SU(2) matrices rather than in terms of classical fixed-length spins (to this respect, appendix B will be also of interest). This representation of the model will allow for an enormous improvement of the numerical stability of the integration of the equations of motion during the Molecular Dynamics part of the HMC algorithm. In section 3, we present the path-integral formulation of the model, and prove its mathematical equivalence with the Hamiltonian one. In section 4, we give details of our implementation of HMC. Section 5 is devoted to consistency checks: we show numerically how our *perfect action* formulation avoids the need for a Trotter-Suzuki extrapolation to continuum Euclidean-time and we compare the numerical results of the HMC simulation with an usual Hamiltonian one. In section 6 we present our results for the PM-FM phase transition at half filling. Section 7 is devoted to conclusions. We also include three appendices with useful formulae and the proofs of some relations used.

2 The model

We consider the lattice Kondo model on a cubic lattice of side L and volume $V = L^3$, where periodic boundary conditions are applied. On each lattice site we have a classical localized spin, $\vec{\phi}_{\boldsymbol{x}}$ of unit-length. The spins interact with a band of lattice fermions through the Hamiltonian

$$\mathcal{H} = \sum_{\boldsymbol{x},\alpha} \sum_{\boldsymbol{y},\beta} c^\dagger_{\boldsymbol{x},\alpha} H_{\boldsymbol{x},\alpha;\boldsymbol{y},\beta} c_{\boldsymbol{y},\beta} \,, \tag{1}$$

where $\boldsymbol{x}$ and $\boldsymbol{y}$ run over all nodes of the spatial lattice, and $\alpha, \beta = 1, 2$ are spin indices. The single-particle Hamiltonian matrix consist of a hopping term plus the Hund coupling with the localized spins:

$$H_{\boldsymbol{x},\alpha;\boldsymbol{y},\beta} = -t \sum_{i=1}^{d} \delta_{\alpha,\beta} \left[\delta_{\boldsymbol{x};\boldsymbol{y}+\boldsymbol{i}} + \delta_{\boldsymbol{x};\boldsymbol{y}-\boldsymbol{i}}\right] - J_H \, \delta_{\boldsymbol{x};\boldsymbol{y}} (\vec{\phi}_{\boldsymbol{x}} \cdot \vec{\sigma})_{\alpha,\beta} \,, \tag{2}$$

where $\boldsymbol{i}$ is the unit vector in the i direction and $\vec{\sigma} = \{\sigma_1, \sigma_2, \sigma_3\}$ are the Pauli matrices. For the particular case of the CMR manganites, the localized spins represent the three core manganese t_{2g} electrons that, due to the Hund rule, yield a $S = 3/2$ spin that for most purposes can be considered as classical. The conduction electrons, represented by the creation and annihilation operators $c_{\boldsymbol{x},\alpha}$, $c^\dagger_{\boldsymbol{x},\alpha}$, occupy the lowest of the two manganese e_g orbitals, split by a Jahn-Teller distortion.

The statistical properties of the system with an explicit superexchange antiferromagnetic coupling between the localized spins can be obtained through the partition function. Choosing units such that $k_{\mathrm{B}} = 1$, the partition function reads

$$Z = \int \mathrm{D}\vec{\phi} \; \mathrm{e}^{-\frac{1}{T} H^{SE}} \; \mathrm{Tr}^{\mathrm{Fock}} \, \mathrm{e}^{-\frac{1}{T}(\mathcal{H} - \mu \mathcal{N})} \,, \tag{3}$$

the superexchange hamiltonian being

$$H^{SE} = J_{\rm AF} \sum_{\boldsymbol{x}} \sum_{i=1}^{d} \vec{\phi}_{\boldsymbol{x}} \cdot \vec{\phi}_{\boldsymbol{x}+\boldsymbol{i}} \,, \tag{4}$$

and $\mathcal{N}$ is the number operator

$$\mathcal{N} = \sum_{\boldsymbol{x},\alpha} c^{\dagger}_{\boldsymbol{x},\alpha} c_{\boldsymbol{x},\alpha} \,, \quad [\mathcal{N}, \mathcal{H}] = 0 \,. \tag{5}$$

The problem can be enormously simplified, due to the non self-interacting nature of the Hamiltonian (1). Although $\mathcal{H}$ is a $4^V \times 4^V$ matrix in the Fock space, the trace in Eq. (3) can be explicitly taken if the eigenvalues of the $2V \times 2V$ single-particle Hamiltonian matrix, $\{E_n\}_{n=1,\ldots,2V}$, are known:

$$\mathrm{Tr}^{\rm Fock}\, \mathrm{e}^{-\frac{1}{T}(\mathcal{H}-\mu\mathcal{N})} = \mathrm{e}^{\sum_n \log\left(1+\mathrm{e}^{-\frac{E_n-\mu}{T}}\right)} \,. \tag{6}$$

It is thus clear that, as we have said in the introduction, the resulting Boltzmann-weight is positive, and that the model can readily be simulated by the Metropolis algorithm, up to the computational caveats mentioned in the previous section. For numerical calculations based on this strategy, see Ref. [5].

The dimensionality of the matrices can be still reduced in a factor of two, in the limit of large Hund coupling, thus obtaining Zener's double-exchange model [2]. One first makes a unitary transformation that diagonalizes the Hund coupling term in Eq. (2):

$$H \;\rightarrow\; \Omega H \Omega^{\dagger} \tag{7}$$

$$\Omega_{\boldsymbol{x},\alpha;\boldsymbol{y}\beta} \;=\; \delta_{\boldsymbol{x},\boldsymbol{y}} U(\vec{\phi}_{\boldsymbol{x}})_{\alpha,\beta} \tag{8}$$

$$U(\vec{\phi}) \;=\; \begin{pmatrix} \cos\dfrac{\theta}{2}\mathrm{e}^{\mathrm{i}(\pi+\varphi)/2} & \sin\dfrac{\theta}{2}\mathrm{e}^{\mathrm{i}(\pi-\varphi)/2} \\ \sin\dfrac{\theta}{2}\mathrm{e}^{\mathrm{i}(\pi+\varphi)/2} & -\cos\dfrac{\theta}{2}\mathrm{e}^{\mathrm{i}(\pi-\varphi)/2} \end{pmatrix} , \tag{9}$$

where θ and φ are respectively the polar and azimuthal angle that determine the spin $\vec{\phi}$ direction. It will also be important in what follows our choosing of $U(\vec{\phi})$ as an SU(2) matrix. The resulting single-particle Hamiltonian matrix is

$$H_{\boldsymbol{x},\alpha;\boldsymbol{y},\beta} = -\, J_H\,(\sigma_3)_{\alpha,\beta} \;- t \sum_{i=1}^{d} \left[\left(U(\vec{\phi}_{\boldsymbol{x}}) U^{\dagger}(\vec{\phi}_{\boldsymbol{y}}) \right)_{\alpha,\beta} \delta_{\boldsymbol{x},\boldsymbol{y}+\boldsymbol{i}} \;+\; \left(U(\vec{\phi}_{\boldsymbol{x}}) U^{\dagger}(\vec{\phi}_{\boldsymbol{y}}) \right)_{\alpha,\beta} \delta_{\boldsymbol{x},\boldsymbol{y}-\boldsymbol{i}} \right] . \tag{10}$$

Due to the largeness of the Hund coupling one should keep only the electron state with spin parallel to its core spin (the "1" state in the representation of Eq. (10)). The truncated single-particle Hamiltonian matrix is then

$$H_{\boldsymbol{x},\boldsymbol{y}} = -t \sum_{i=1}^{d} \left[\left(U(\vec{\phi}_{\boldsymbol{x}}) U^{\dagger}(\vec{\phi}_{\boldsymbol{x}-\boldsymbol{i}}) \right)_{1,1} \delta_{\boldsymbol{x},\boldsymbol{y}+\boldsymbol{i}} \;+\; \left(U(\vec{\phi}_{\boldsymbol{x}}) U^{\dagger}(\vec{\phi}_{\boldsymbol{x}+\boldsymbol{i}}) \right)_{1,1} \delta_{\boldsymbol{x},\boldsymbol{y}-\boldsymbol{i}} \right] . \tag{11}$$

Let us take a look at the product

$$\left(U(\phi_{\boldsymbol{x}}) U^{\dagger}(\phi_{\boldsymbol{y}}) \right)_{1,1} = \mathrm{e}^{\mathrm{i}\varphi_{\boldsymbol{x}}/2} \left[\cos\frac{\theta_{\boldsymbol{x}}}{2} \cos\frac{\theta_{\boldsymbol{y}}}{2} \;+\; \sin\frac{\theta_{\boldsymbol{x}}}{2} \sin\frac{\theta_{\boldsymbol{y}}}{2}\, \mathrm{e}^{-\mathrm{i}(\varphi_{\boldsymbol{x}}-\varphi_{\boldsymbol{y}})} \right] \mathrm{e}^{-\mathrm{i}\varphi_{\boldsymbol{y}}/2} \,. \tag{12}$$

The term between square brackets is nothing but the hopping term of the DEM model (see e.g. [7]). Thus we see that the matrix in Eq. (11) is actually an unitary-transformed of the usual hopping term, the unitary transformation being

$$\tilde{\Omega}_{\boldsymbol{x}\boldsymbol{y}} = \delta_{\boldsymbol{x},\boldsymbol{y}} \mathrm{e}^{\mathrm{i}\varphi_{\boldsymbol{x}}/2} \,. \tag{13}$$

Now, the expression in Eq. (11) is extremely more convenient for an HMC study than the usual one. In fact, during the Molecular Dynamics part of the algorithm, one needs to take care of the constraint

$(\vec{\phi}_{\boldsymbol{x}})^2 = 1$. It can be done with a modification of the usual equation of motions as shown in Ref. [9]. To get these new equations of motion one needs to express the hopping term of the DEM in terms of the Cartesian coordinates of the spin (ϕ^1, ϕ^2, ϕ^3)

$$\cos\frac{\theta_{\boldsymbol{x}}}{2}\cos\frac{\theta_{\boldsymbol{y}}}{2} \;+\; \sin\frac{\theta_{\boldsymbol{x}}}{2}\sin\frac{\theta_{\boldsymbol{y}}}{2}\,\mathrm{e}^{-\mathrm{i}(\varphi_{\boldsymbol{x}}-\varphi_{\boldsymbol{y}})} = \frac{1}{2}\left(\sqrt{1+\phi^3_{\boldsymbol{x}}}\sqrt{1+\phi^3_{\boldsymbol{y}}} + \frac{(\phi^1_{\boldsymbol{x}}-\mathrm{i}\phi^2_{\boldsymbol{x}})(\phi^1_{\boldsymbol{y}}+\mathrm{i}\phi^2_{\boldsymbol{y}})}{\sqrt{1+\phi^3_{\boldsymbol{x}}}\sqrt{1+\phi^3_{\boldsymbol{y}}}}\right). \quad (14)$$

Indeed, a working HMC algorithm can be obtained using the above representation [9], which is not analytic at the sphere South Pole. However, during the Molecular Dynamics step of the HMC, one needs the derivatives of the right-hand side of Eq. (14), which at the South Pole are even more singular than (14), resulting on a poor numerical stability of the integration of the equation of motion. On the contrary, the expression of the hopping term as a function of the SU(2) matrices is smooth. Moreover, as discussed in Appendix B, nothing changes if we substitute the integrations over the spin-field in the partition function, by an integration over the SU(2) group. If needed, the spins $\vec{\phi}_{\boldsymbol{x}}$ can be obtained from the SU(2) matrices using the formula (see appendix B)

$$\phi^j_{\boldsymbol{x}} = \frac{1}{2}\mathrm{Tr}\left(\sigma_j U^\dagger_{\boldsymbol{x}}\sigma_3 U_{\boldsymbol{x}}\right)\,,\; j=1,2,3\,. \quad (15)$$

Thus we will consider the following statistical system, which is strictly equivalent to Eq. (3) in the double-exchange limit:

$$Z = \int DU \mathrm{e}^{-\frac{1}{T}H^{SE}+\sum_{n=1}^{V}\log\left(1+\mathrm{e}^{-\frac{E_n-\mu}{T}}\right)}\,, \quad (16)$$

$$H^{SE} = \frac{J_{\mathrm{AF}}}{2}\sum_{\boldsymbol{x}}\sum_{i=1}^{d}\mathrm{Tr}\left[(U^\dagger_{\boldsymbol{x}}\vec{\sigma}U_{\boldsymbol{x}})\cdot(U^\dagger_{\boldsymbol{x}+\boldsymbol{i}}\vec{\sigma}U_{\boldsymbol{x}+\boldsymbol{i}})\right]. \quad (17)$$

In the above expression, T is the temperature and E_n are the eigenvalues of the single-particle Hamiltonian matrix defined in Eq. (11).

Although the SU(2) field $U_{\boldsymbol{x}}$ is still a constrained variable, it can be dealt with using well established techniques from lattice-gauge theory [10].

Let us also finally mention that the single-particle Hamiltonian Eq. (11), is unitary equivalent to *minus* itself, the unitary transformation being (x, y, z are the lattice coordinates of $\boldsymbol{x}$)

$$U_{\boldsymbol{x},\boldsymbol{y}} = \delta_{\boldsymbol{x},\boldsymbol{y}}(-1)^{x+y+z} \quad (18)$$

This ensures that the spectrum is symmetric around zero and therefore half-filling corresponds to $\mu = 0$.

3 From the Hamiltonian to the Path-Integral formulation

In this section, we will show how to obtain a numerically tractable path integral representation of the partition function (16) although our results will be valid for the general problem outlined in the introduction: classical continuous degrees of freedom coupled to non self-interacting fermions. In subsection 3.1 we shall also explain how some important fermionic observables can be recovered in this formalism.

Let us first state the following well known expression for the partition function in terms of a pair of anticonmuting Grassman fields $\{\Psi^\dagger_{\boldsymbol{x}}(\tau), \Psi_{\boldsymbol{x}}(\tau)\}$, where τ is the Euclidean time [13],

$$Z = \int DU\, D\Psi\, D\Psi^\dagger \mathrm{e}^{-S_{\mathrm{F}}-\frac{1}{T}H^{SE}}\,, \quad (19)$$

$$S_F = \int_0^{\frac{\hbar}{T}} d\tau\left[\sum_{\boldsymbol{x}}\Psi^\dagger_{\boldsymbol{x}}\frac{\partial\Psi_{\boldsymbol{x}}}{\partial\tau} - \frac{1}{\hbar}\sum_{\boldsymbol{x},\boldsymbol{y}}\Psi^\dagger_{\boldsymbol{x}}(H_{\boldsymbol{x},\boldsymbol{y}}-\mu\delta_{\boldsymbol{x},\boldsymbol{y}})\Psi_{\boldsymbol{y}}\right]. \quad (20)$$

In the above expressions, H is the single-particle matrix defined in Eq. (11), and the Grassman fields verify antiperiodic boundary conditions in the Euclidean-time direction

$$\Psi^\dagger_{\boldsymbol{x}}(0) = -\Psi^\dagger_{\boldsymbol{x}}(\hbar/T) \quad , \quad \Psi_{\boldsymbol{x}}(0) = -\Psi_{\boldsymbol{x}}(\hbar/T)\,. \quad (21)$$

Now, in order to transform the representation (20) onto a numerically tractable problem, we introduce a time discretization. We introduce L_τ time slices (for technical reasons, L_τ will always be an even number, see Eq. (37)), with a spacing a_τ such that

$$L_\tau a_\tau = \frac{\hbar}{T} \,. \tag{22}$$

In this way, instead of a three-dimensional lattice and a continuum time, we have a four dimensional lattice. The Grassman fields now depend on the discrete coordinate x_τ,

$$\tau = x_\tau a_\tau \quad , \quad x_\tau = 0, 1, \ldots, L_\tau - 1 \,, \tag{23}$$

and verify the boundary conditions

$$\Psi^\dagger_{0,\boldsymbol{x}} = -\Psi^\dagger_{L_\tau,\boldsymbol{x}} \quad , \quad \Psi_{0,\boldsymbol{x}} = -\Psi_{L_\tau,\boldsymbol{x}} \,. \tag{24}$$

The fields $U_{\boldsymbol{x}}$ instead, being classical, do not depend on Euclidean time. In order to check how close our time discretization is from the continuous limit of Eq. (20), we need to compare a_τ with the natural time unit of our problem, $\hbar/t$ (see Eq. (11)). Therefore, the dimensionless parameter that controls how close we are to the continuum-time limit is

$$\lambda = \frac{a_\tau t}{\hbar} \,. \tag{25}$$

Our discretization should be such that in the $\lambda \to 0$ limit Eq. (20) is recovered, much in the spirit of the Trotter-Suzuki extrapolation. From now on let us also adopt the convention that the quantities with dimension of energy, $T, \mu, J_{\rm AF}$ and the matrix H are measured in units of t, in such a way that for instance

$$T = \frac{1}{\lambda L_\tau} \,. \tag{26}$$

With all our notational conventions settled, the discretized form of the action is

$$S^\lambda_{\rm F} = \sum_{x_\tau,\boldsymbol{x}} \mathrm{e}^{\mu\lambda} \Psi^\dagger_{x_\tau,\boldsymbol{x}} \Psi_{x_\tau+1,\boldsymbol{x}} - \sum_{x_\tau,\boldsymbol{x},\boldsymbol{y}} \Psi_{x_\tau,\boldsymbol{x}} \left[\exp(\lambda H)\right]_{\boldsymbol{x};\boldsymbol{y}} \Psi_{x_\tau,\boldsymbol{y}} \tag{27}$$

$$\equiv \sum_{x_\tau,\boldsymbol{x}} \sum_{y_\tau,\boldsymbol{y}} \Psi^\dagger_{x_\tau,\boldsymbol{x}} M^\lambda_{x_\tau,\boldsymbol{x};y_\tau,\boldsymbol{y}} \Psi_{y_\tau,\boldsymbol{y}} \,. \tag{28}$$

The last equality on the above expressions defines the so called fermionic matrix M^λ. The rationale for including the chemical potential on the temporal *link* that joins the $(x_\tau, \boldsymbol{x})$ site with the $(x_\tau + 1, \boldsymbol{x})$ one, can be found in Refs. [14]. It is easy to check that in the $\lambda \to 0$ limit the continuum-time action is recovered. The exponential form in the spatial part of Eq. (27) is preferred over more straightforward ones because it yields a *perfect* action, as shown below, without any time discretization effect. For the particular case of the DEM model, the action in Eq. (27) can be directly simulated. For other models, the approximated form

$$\left[\exp(\lambda H)\right]_{\boldsymbol{x};\boldsymbol{y}} \approx \delta_{\boldsymbol{x};\boldsymbol{y}} \;+\; \lambda\, H_{\boldsymbol{x};\boldsymbol{y}} \,, \tag{29}$$

could be the only feasible one, but it would makes mandatory to consider the $\lambda \to 0$ extrapolation.

To show the correctness of our path-integral, it is useful to first introduce the time Fourier transformed field,

$$\Psi_{x_\tau,\boldsymbol{x}} = \frac{1}{\sqrt{L_\tau}} \sum_{p_\tau} \mathrm{e}^{i p_\tau x_\tau} \Psi_{p_\tau,\boldsymbol{x}} \;, \tag{30}$$

where the sum extends over the Matsubara frequencies (see Eq. (24)),

$$p_0 = \frac{2\pi}{L_\tau} q \,, \quad q = -\frac{L_\tau - 1}{2}, \ldots, -\frac{1}{2}, \frac{1}{2}, \ldots, \frac{L_\tau - 1}{2} \,. \tag{31}$$

The fermionic action now reads

$$S^\lambda_{\rm F} = \sum_{p_0,\boldsymbol{x}} \mathrm{e}^{\mu\lambda + i p_0} \Psi^\dagger_{p_0,\boldsymbol{x}} \Psi_{p_0,\boldsymbol{x}} - \sum_{p_0,\boldsymbol{x},\boldsymbol{y}} \Psi^\dagger_{p_0,\boldsymbol{x}} \left[\exp(\lambda H)\right]_{\boldsymbol{x};\boldsymbol{y}} \Psi_{p_0,\boldsymbol{y}} \,. \tag{32}$$

Therefore, the fermionic matrix defined in Eq. (28) is block-diagonal in this basis

$$M^{\lambda}_{p_0,\boldsymbol{x};p_0',\boldsymbol{y}} = \delta_{p_0,p_0'} A_{\boldsymbol{x};\boldsymbol{y}}(p_0,\lambda)\,, \tag{33}$$

$$A_{\boldsymbol{x};\boldsymbol{y}}(p_0,\lambda) = \mathrm{e}^{\mu\lambda+ip_0}\delta_{\boldsymbol{x},\boldsymbol{y}} - [\exp(\lambda H)]_{\boldsymbol{x};\boldsymbol{y}}\,, \tag{34}$$

and the Hamiltonian matrix, being Hermitian, verifies

$$A^{\dagger}(p_0,\lambda) = A(-p_0,\lambda)\,. \tag{35}$$

The partition function is then (using the Grassman version of Gaussian integration)

$$Z^{\lambda} = \int \prod_{\boldsymbol{x}} \mathrm{d}U_{\boldsymbol{x}} \prod_{q_0,\boldsymbol{y}} \mathrm{d}\Psi_{q_0,\boldsymbol{y}} \prod_{p_0,\boldsymbol{x}} D\Psi^{\dagger}_{p_0,\boldsymbol{x}}\, \mathrm{e}^{-\frac{H^{SE}}{T} - \sum_{p_0,\boldsymbol{w}} \sum_{q_0,\boldsymbol{y}} \Psi^{\dagger}_{p_0,\boldsymbol{w}} M^{\lambda}_{p_0,\boldsymbol{w};q_0,\boldsymbol{y}} \Psi_{q_0,\boldsymbol{y}}}\,, \tag{36}$$

$$= \int DU\, \det\left[M^{\lambda}\right] \mathrm{e}^{-\frac{1}{T}H^{SE}} = \int DU \prod_{p_0>0} \det\left[A^{\dagger}(p_0,\lambda)A(p_0,\lambda)\right] \mathrm{e}^{-\frac{H^{SE}}{T}}\,. \tag{37}$$

It is then clear that the block-diagonal from of the fermionic matrix yields a positive-definite Boltzmann weight. Now, in order to relate this Boltzmann weight and our target expressed in Eq. (16), let us first notice that the eigenvalues of the $A(p_0)$, in terms of the V eigenvalues of the Hamiltonian single-particle matrix (11), are

$$E^{A}_{n}(\lambda,p_0) = \mathrm{e}^{\mu\lambda+ip_0} - \mathrm{e}^{\lambda E_n}\,. \tag{38}$$

Now using the equation

$$\prod_{p_0} \left(\mathrm{e}^{\mu\lambda+ip_0} - \mathrm{e}^{\lambda E}\right) = \mathrm{e}^{\log\left(1+\mathrm{e}^{-\frac{E-\mu}{T}}\right)+\frac{E}{T}}\,, \tag{39}$$

proved in appendix A, we find for the fermionic determinant

$$\det\left[M^{\lambda}\right] = \prod_{n}\prod_{p_0} \left(\mathrm{e}^{\mu\lambda+ip_0} - \mathrm{e}^{\lambda E_n}\right)\,, \tag{40}$$

$$= \mathrm{e}^{\sum_n \left[\log\left(1+\mathrm{e}^{-\frac{E_n-\mu}{T}}\right)+\frac{E_n}{T}\right]}\,, \tag{41}$$

$$= \mathrm{e}^{\frac{1}{T}\mathrm{Tr}H + \sum_n \left[\log\left(1+\mathrm{e}^{-\frac{E_n-\mu}{T}}\right)\right]}\,. \tag{42}$$

Since the single-particle Hamiltonian matrix (11) is traceless, it is clear that the discretized action exactly reproduces the target Boltzmann-weight (16) and thus it can be rightly called a *perfect action*. In the general case, though, one would have to take out by hand the $\mathrm{Tr}H/T$ from the Boltzmann weight.

Before ending-up, let us say a few words about the (in principle) non local matrix $\exp[\lambda H]$. In a model such as the DEM, where the eigenvalues of the single-particle Hamiltonian matrix are within some *a priori* known bounds, it can be numerically computed with a polynomial expansion as described in appendix C. In other cases, although the energy must be bounded from below if the system is to be stable, an upper bound may not be available. Then one will be enforced to use an approximation such as Eq. (29). It would anyway be convenient to add a multiple of the identity matrix to the single-particle Hamiltonian, in order to have a positive spectrum. From the above analysis, it follows that with the approximation Eq. (29), the simulation would be exact for the λ dependent single-particle Hamiltonian

$$H^{\lambda} = \frac{1}{\lambda}\log(1+\lambda H)\,. \tag{43}$$

Therefore, there would be a deformation of the spectrum (as one finds using the Trotter-Suzuki formula at finite time-slicing), that would disappear on the $\lambda \to 0$ limit. More bothersome, there would be an *empty-band* dynamical effect. Indeed, even in the $\mu \to -\infty$ limit, where fermions should not influence the classical degrees of freedom, the $\mathrm{Tr}H^{\lambda}$ term of Eq. (42) would be present, and as one has

$$\frac{1}{\lambda}\log(1+\lambda H) = H - \frac{\lambda}{2}H^2 + \ldots\,, \tag{44}$$

the spins would definitively feel this spurious interaction, even if $\mathrm{Tr}H = 0$. One can completely cure this problem, by using the Boltzmann-weight

$$Z = \int DU \prod_{p_0>0} \det \left[\frac{A^\dagger(p_0,\lambda,\mu)A(p_0,\lambda,\mu)}{A^\dagger(p_0,\lambda,\mu=-\infty)A(p_0,\lambda,\mu=-\infty)} \right] \mathrm{e}^{-\frac{H^{SE}}{T}} , \tag{45}$$

that can be simulated, using a straightforward modification of the HMC algorithm explained in section 4, because the matrices $A(p_0,\mu)$ commute for all values of p_0, λ and μ.

3.1 Fermionic Operators

3.1.1 Charge density

Let us call $|\boldsymbol{x}\rangle$ the state localized on the lattice site $\boldsymbol{x}$, and $|n\rangle$ the eigenvector of the single-particle Hamiltonian matrix (11) corresponding to the eigenvalue E_n. The charge density on site $\boldsymbol{x}$, for the given configuration of the spin-field is

$$\rho_{\boldsymbol{x}} = \sum_{n=1}^{V} |\langle n|\boldsymbol{x}\rangle|^2 \frac{1}{\mathrm{e}^{\frac{E_n-\mu}{T}}+1} , \tag{46}$$

while the average charge-density on the lattice is

$$\rho \equiv \frac{1}{V}\sum_{\boldsymbol{x}} \rho_{\boldsymbol{x}} = \frac{1}{V}\sum_{n} \frac{1}{\mathrm{e}^{\frac{E_n-\mu}{T}}+1} . \tag{47}$$

Now, using (see appendix A)

$$\frac{1}{L_\tau}\sum_{p_0} \frac{e^{\mu\lambda+ip_0}}{\mathrm{e}^{\mu\lambda+ip_0}-\mathrm{e}^{\lambda E}} = \frac{1}{1+\mathrm{e}^{\frac{E-\mu}{T}}} \tag{48}$$

we obtain

$$\rho_{\boldsymbol{x}} = \frac{1}{L_\tau}\sum_{p_0} \mathrm{e}^{\lambda\mu+\mathrm{i}p_0} \sum_n \frac{|\langle n|\boldsymbol{x}\rangle|^2}{\mathrm{e}^{\lambda\mu+\mathrm{i}p_0}-\mathrm{e}^{\lambda E_n}} = \frac{1}{L_\tau}\sum_{p_0} \mathrm{e}^{\lambda\mu+\mathrm{i}p_0} \left[A(p_0,\lambda)\right]^{-1}_{\boldsymbol{x},\boldsymbol{x}} , \tag{49}$$

while

$$\rho = \frac{1}{V}\frac{1}{L_\tau}\sum_{p_0} \mathrm{e}^{\lambda\mu+\mathrm{i}p_0} \mathrm{Tr}\left[A(p_0,\lambda)\right]^{-1} . \tag{50}$$

In practice, we make use of the equality between the thermal average of $\rho_{\boldsymbol{x}}$ and the one of ρ, since most of computer-time during a HMC simulation is spent in the inversion of the matrices $A(p_0,\lambda)$, which is done row-by-row. We therefore only calculate one row of the inverse matrix, and store the corresponding value of $\rho_{\boldsymbol{x}}$.

3.1.2 Fermionic Energy

In the Hamiltonian formalism the energy (per spin) for a given configuration of the spin degrees of freedom, is obtained from the logarithmic derivative with respect to the inverse temperature, β, of the partition function, and has the form

$$e = \frac{1}{V}\sum_{n} \frac{E_n-\mu}{\mathrm{e}^{\frac{E_n-\mu}{T}}+1} + \frac{1}{V}H^{SE} . \tag{51}$$

Using again Eq. (48), we can write the first term of the RHS of the previous equation as

$$e_{\mathrm{F}} = \frac{1}{VL_\tau}\sum_{p_0} \mathrm{e}^{\lambda\mu+\mathrm{i}p_0} \sum_n \frac{E_n-\mu}{\mathrm{e}^{\mu\lambda+\mathrm{i}p_0}-e^{\lambda E_n}} , \tag{52}$$

and thus

$$e_{\mathrm{F}} = \frac{1}{L_\tau}\sum_{p_0} \mathrm{e}^{\lambda\mu+\mathrm{i}p_0} \frac{1}{V}\mathrm{Tr}\left[(H-\mu)A^{-1}(p_0,\lambda)\right] . \tag{53}$$

As in the case of the density, one cannot afford to calculate the full trace, but rely on the translational invariance and calculate

$$e_{\rm F}(\boldsymbol{x}) = \frac{1}{L_\tau} \sum_{p_0} {\rm e}^{\lambda\mu + {\rm i}p_0} \left[(H-\mu) A^{-1}(p_0,\lambda) \right]_{\boldsymbol{x},\boldsymbol{x}} \; , \tag{54}$$

that can be readily obtained once the $\boldsymbol{x}^{\rm th}$ row of the matrix $A(p_0,\lambda)$ is known from the density calculation.

On the other hand, the total specific heat cannot be calculated in a practical way from the thermal fluctuation of the energy. Indeed, one can easily find that

$$-\frac{\partial \langle e \rangle}{\partial \beta} = V \left(\left\langle \frac{\partial e_F}{\partial \beta} + e^2 \right\rangle - \langle e \rangle^2 \right) . \tag{55}$$

A representation analogous to Eq. (54) can be readily obtained for $\partial e_{\rm F}/\partial\beta$. The real problem is the calculation of $\langle e^2 \rangle$, because we do not know $e_{\rm F}$, but $e_{\rm F}(\boldsymbol{x})$. It is easy to convince oneself that to substitute $e_{\rm F}$ by $e_{\rm F}(\boldsymbol{x})$ on the calculation of $\langle e^2 \rangle$ produces a systematic overestimation, magnified by the V prefactor.

4 Our implementation of HMC

In this section, we will give the necessary details about our implementation of the HMC algorithm [6]. The reader interested in a full exposition of the algorithm may consult [10].

Let us recall that we want to simulate the statistical system

$$\int DU \prod_{p_0>0} \det \left[A^\dagger(p_0,\lambda) A(p_0,\lambda) \right] \, {\rm e}^{-\frac{H^{SE}}{T}} \, . \tag{56}$$

As usual, the first step is to get rid of the fermionic determinant by using Gaussian integration, introducing the $L_\tau/2$ pseudofermionic (commuting) fields, $\varphi_{p_0,\boldsymbol{x}}$:

$$\det M^\lambda = \int \left(\prod_{p_0>0,\boldsymbol{x}} {\rm d}\varphi_{p_0,\boldsymbol{x}} \right) \left(\prod_{p_0>0,\boldsymbol{x}} {\rm d}\varphi^*_{p_0,\boldsymbol{x}} \right) \exp \left\{ - \sum_{p_0>0,\boldsymbol{x},\boldsymbol{y}} \varphi^*_{p_0,\boldsymbol{x}} (A^\dagger(p_0,\lambda) A(p_0,\lambda))^{-1}_{\boldsymbol{x},\boldsymbol{y}} \varphi_{p_0 \boldsymbol{y}} \right\} . \tag{57}$$

In our case of constrained variables belonging to the SU(2) group, one introduces 3V *momenta* (one per group generator and per lattice site [15]), by multiplying Eq. (37) by unity written in the form

$$1 = \int_{-\infty}^{\infty} \prod_{\boldsymbol{x}} \frac{{\rm d}\vec{P}_{\boldsymbol{x}}}{(2\pi)^{3/2}} \, \exp \left[-\frac{\vec{P}^2_{\boldsymbol{x}}}{2} \right] . \tag{58}$$

So we end-up with a classical-mechanics model, that can be studied using the Molecular Dynamics method. In this model the *kinetic* energy is

$$\mathcal{T} = \sum_{\boldsymbol{x}} \frac{1}{2} \vec{P}^2_{\boldsymbol{x}} \, , \tag{59}$$

while the *potential* one is

$$\mathcal{U} = \frac{H^{SE}}{T} + \sum_{p_0>0,\boldsymbol{x},\boldsymbol{y}} \varphi^*_{p_0,\boldsymbol{x}} (A^\dagger(p_0,\lambda) A(p_0,\lambda))^{-1}_{\boldsymbol{x},\boldsymbol{y}} \varphi_{p_0 \boldsymbol{y}} \, . \tag{60}$$

Following the standard procedure, at the beginning of each Molecular Dynamics trajectory, the momenta are extracted with the corresponding Gaussian probability (58), while the pseudofermions are obtained from a Gaussian vector $\xi_{p_0,\boldsymbol{x}}$ as

$$\varphi_{p_0} = A^\dagger(p_0,\lambda) \xi_{p_0} \, . \tag{61}$$

In practice, the pseudofermions being instantaneously thermalized, they are not changed during the trajectory. It is useful to consider instead two molecular-dynamics time dependent fields

$$\eta = (A^\dagger A)^{-1}\varphi\,, \tag{62}$$

$$\xi = A\eta\,, \tag{63}$$

Although φ is not changing, the matrix $A(p_0,\lambda)$ changes when the field $U_{\boldsymbol{x}}$ follows the dynamic. The equations of motion adapted to the SU(2) group constraints are [15] (the $\partial_{\boldsymbol{x},j}$ derivative is defined in appendix B).

$$\dot{U}_{\boldsymbol{x}} = \left(\mathrm{i}\vec{P}_{\boldsymbol{x}}\cdot\vec{\sigma}\right)U_{\boldsymbol{x}}\,, \tag{64}$$

$$\dot{P}_{\boldsymbol{x},j} = -\partial_{\boldsymbol{x},j}\mathcal{U}\,. \tag{65}$$

The hard part to calculate is of course

$$\begin{aligned}\partial_{\boldsymbol{x},j}\left(\varphi^\dagger(A^\dagger A)^{-1}\varphi\right) &= -\varphi^\dagger(A^\dagger A)^{-1}\left[(\partial_{\boldsymbol{x},j}A^\dagger)A + A^\dagger\partial_{\boldsymbol{x},j}A\right](A^\dagger A)^{-1}\varphi \\ &= -\eta^\dagger(\partial_{\boldsymbol{x},j}A^\dagger)\xi - \xi(\partial_{\boldsymbol{x},j}A)\eta = -2\mathrm{Re}\left[\xi^\dagger(\partial_{\boldsymbol{x},j}A)\eta\right]\end{aligned} \tag{66}$$

Thus we see that a knowledge of the full inverse $A(p_0,\lambda)$ matrices is useless, and it is enough to consider the field η defined in Eq. (62). Once we know how to calculate derivatives of the exponential of the single-particle matrix (see appendix C), the rest of the calculation is standard: we numerically integrate the equations of motion by means of the SU(2) leap-frog algorithm [15], inverting the $A(p_0,\lambda)$ matrices using a conjugate-gradient method. A numerical trick of some relevance is that one can calculate the inverses during the Molecular-Dynamics steps of the algorithm with far less accuracy than during the Monte Carlo accept-reject step [9, 16]. For the exponential of the single-particle Hamiltonian, we have used an order of the polynomial expansion such that the error is smaller than 2×10^{-4} all over the spectrum.

An important remark about the algorithm is that pseudofermionic (four dimensional) variables φ can be straightforwardly generated following the exact probability distribution. This allows to simulate systems very long in the time direction without compromising the autocorrelation time.

5 Consistency checks

We consider in this section some tests performed to check the algorithm. Firstly, we should mention that although the computer code for the HMC is rather complex, most of the routines are very easy to check. For instance, the matrix inversion is self consistent, and the integration of the equations of motion can be directly checked as they should conserve the Molecular Dynamics Hamiltonian (up to second order in the leap-frog step). In addition, we have checked explicitly the reversibility of the equations of motion.

A posteriori, it is very useful to control the Creutz parameter[17] defined as

$$\langle \mathrm{e}^{-\Delta H_{\mathrm{MD}}}\rangle\,, \tag{67}$$

where all variations of H_{MD} must be considered (accepted or not). This quantity should be 1, and its measure is a very strong check of the simulation. A deviation would mean a reversibility problem or a lack of equilibration. We have readily checked this parameter in all the simulations.

Regarding the comparison of the time discretized model with the physical continuous limit target, we have performed the following two types of test. On the first place, we have simulated a 4^3 lattice at $T=1/8$, for decreasing values of λ, using Eq.(29), with a shift of the identity 6λ that ensures a positive spectrum. The empty-band dynamical effect is avoided using Eq.(45). We have chosen $\mu=-3.5$ and $J_{\mathrm{AF}}=0$ which, for $T=1/8$ is near the Paramagnetic-Ferromagnetic transition. The results are displayed in Fig. 1 for several quantities. For this selection of the parameters a linear behavior in λ is observed only for large values of $L_\tau=(T\lambda)^{-1}$. We have also carried out a simulation with the Perfect Action (see appendix C) in a $4^3\times16$ lattice at $\lambda=0.25$ with a 6 degree polynomial approximation. The result is

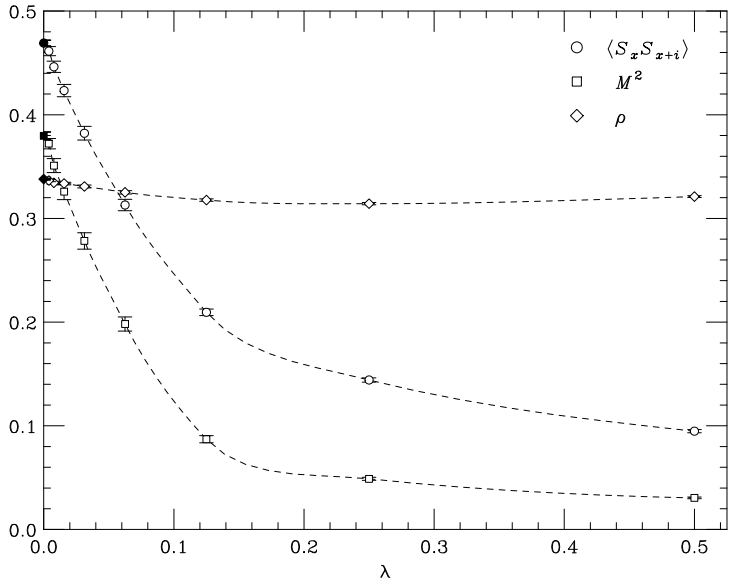


Figure 1: Continuous time limit for the nearest neighbor correlation, magnetization squared and charge density in a 4^3 lattice at $J_{\rm AF}/t = 0$, $T = 1/8$, $\mu = -0.35$. The left-most open symbols require $L_\tau = 2048$. The filled symbols correspond to a simulation with the Perfect Action (109) using $\lambda = 0.25$, $L_\tau = 32$.

$J_{\rm AF}/t$		-0.01	0.05	0.2	0.3
$\langle S_{\boldsymbol{x}} \cdot S_{\boldsymbol{x}+\boldsymbol{i}} \rangle$	Hamiltonian	0.7734(8)	0.3817(18)	$-0.4699(5)$	$-0.6842(5)$
	HMC	0.7717(10)	0.3838(8)	$-0.4697(3)$	$-0.6852(4)$
$(\vec{M})^2$	Hamiltonian	0.7149(16)	0.0162(7)	0.0130(4)	0.3580(13)
	HMC	0.7127(16)	0.0152(3)	0.01340(16)	0.3611(11)

Table 1: Comparison of the results of Hamiltonian and HMC simulations in L^3 lattice with $T = 1/20$ at half filling ($\mu = 0$). We show the correlation between nearest neighbor spins and the square of the magnetization (magnetization staggered when that correlation is negative). The numbers correspond to 10000 measures in each case.

plotted as filled symbols in Fig. 1. The agreement is excellent. The selection of λ for a Perfect Action simulation should be taken looking at the performance of the algorithm. Most of the results presented in this article have been obtained with $\lambda = 0.125$ and a polynomial degree of 6. Larger values of λ have the advantage of requiring smaller values of L_τ but the matrix inversion is more expensive. Conversely, smaller values of λ require larger L_τ while the benefit in the matrix inversion is scarce.

Our second test, and maybe the strongest proof of the HMC method and of our implementation of it is a direct comparison with numerical results from a Hamiltonian simulation. The Hamiltonian model was defined in terms of spins rather than SU(2) matrix, in order to provide a full proof of equivalence. We have carried simulations with both algorithms with the same parameters. We have chosen a 4^3 lattice at $T = 1/20$ for several values of the antiferromagnetic coupling to go over the different phases of the system. Some of the measures are presented in Table 1. We observe a perfect agreement with precisions up to a few per thousand.

6 Numerical results.

In this section we present the results of our HMC simulation using the perfect action in the region of the Paramagnetic–Ferromagnetic phase transition at vanishing superexchange coupling. We have chosen a

fixed temporal length $L_\tau = 40$ varying the temperature through a λ variation.

For simplicity on the analysis, we have restricted ourselves to the half-filling case. Due to the hole-particle symmetry of the DEM, this can be ensured by setting the chemical potential to zero (see Eq.(18)). The study of other band-fillings requires to carefully tune the chemical potential, and will be left for further work.

We have simulated in lattices of spatial sizes $L = 4, 6, 8, 12, 16$ for several values of the temperature. We measure every HMC trajectory discarding up to 600 for thermalization (in the worst case). We collect between 1000 and 10000 measures at every point. We display our results for the spin magnetization (squared) in Fig. 2. The time needed for a trajectory in a 500 MHz Pentium III is about six minutes for a 12^3 lattice in the critical region with 25 leap frog steps of size 0.02.

Let us first define the measured observables, and show their general temperature and lattice-size evolution, and then later consider in detail their behavior close to the critical region, and measure the critical exponents.

The observables are best defined in terms of the correlation function (the $\langle\cdot\rangle$ stands for Boltzmann average,

$$G(\boldsymbol{x}) = \frac{1}{V}\sum_{\boldsymbol{y}} \langle \vec{\phi}_{\boldsymbol{y}} \cdot \vec{\phi}_{\boldsymbol{y}+\boldsymbol{x}} \rangle \,, \tag{68}$$

and its Fourier transform, $\hat{G}(\boldsymbol{k})$. Then the susceptibility is proportional to the squared magnetization:

$$\chi = \hat{G}(\boldsymbol{k}=0) = V\langle M^2 \rangle \tag{69}$$

It is also very useful to consider a finite-lattice correlation-length, in terms of the minimum allowed momentum in a finite lattice [19], $\boldsymbol{k}_{\min} = (2\pi/L, 0, 0)$

$$\xi = \frac{1}{2\sin(k_{\min})}\left(\frac{\chi}{\hat{G}(\boldsymbol{k}_{\min})} - 1\right)^{1/2} \tag{70}$$

Notice that the above definitions use non-connected correlation functions, and therefore the above correlation-length diverges in the ferromagnetic phase like $\mathcal{O}(L^{1+D/2})$. In the thermodynamic limit, ξ diverges at the critical point like $|t|^{-\nu}$, (t is the reduced temperature). The critical behavior for χ is $|t|^{-\gamma}$.

In Fig. 2 we show the temperature and lattice size evolution of M^2. There are several features to be noted. The first one is that the behavior of the $L = 4$ lattice is rather pathological. We believe that this evidences better than any other example the need for larger lattices simulations of spin-fermion models. It is also interesting to notice the larger lattices rapidly tend to their thermodynamical limit, out from the critical region. Finally, we observe that the low temperature behavior of M^2 is linear. This can be readily understood if we set that the average direction of the magnetization is, say, the third axis. In that case,

$$M^2 = 1 - \frac{1}{V}\sum_{\boldsymbol{x}} \langle (\phi^1_{\boldsymbol{x}})^2 + (\phi^2_{\boldsymbol{x}})^2 \rangle + \mathcal{O}((\phi^1)^4, (\phi^2)^4, (\phi^1\phi^2)^2) \,. \tag{71}$$

Since the deviations from the perfect ferromagnetic order are proportional to the mean value of a quadratic operator, the linear behavior with temperature follows from the equipartition principle, that holds for our *classical* spins at low temperatures.

In Fig. 3 we show the correlation-length in units of the lattice size. Notice that the curves for the different lattices cross at a temperature growing with growing lattice-size. Eventually the crossings should occur at the critical point, as dictated by the Finite-Size Scaling Ansatz (see next section). One can also observe that ξ/L is a growing function of the lattice size in the ferromagnetic phase, as it should be.

6.1 Critical Exponents

The main question of interest is whether the DEM presents a second order phase transition between the paramagnetic phase and the ferromagnetic one, at finite temperature. If the answer is positive, one may also wonder about the Universality Class of this phase transition [20]. In principle, one of the two following scenarios should hold:

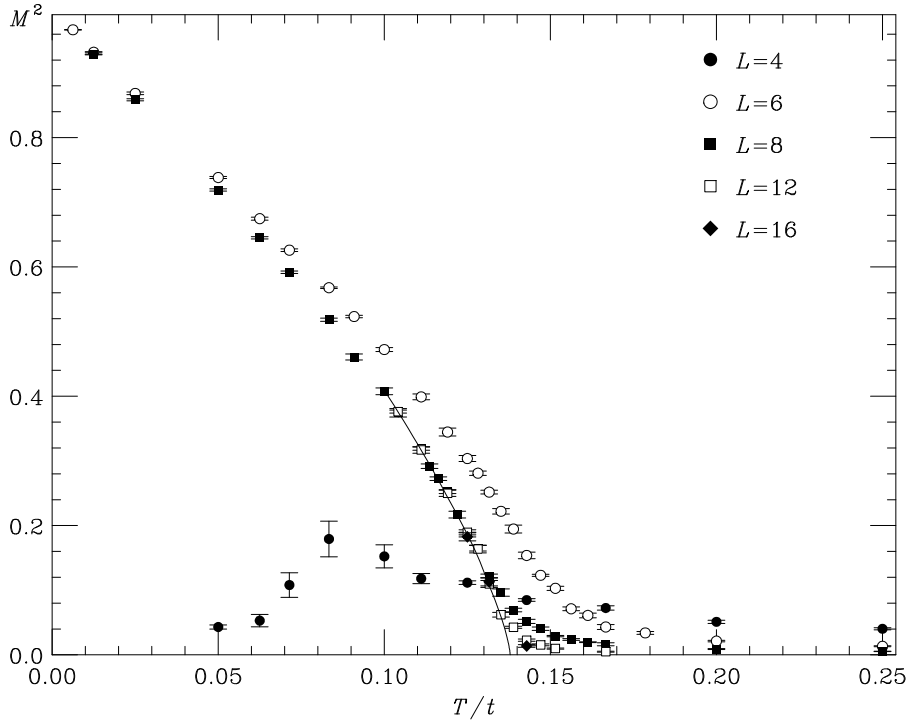


Figure 2: Magnetization squared as a function of the temperature at $J_{\rm AF} = 0$, $\rho = 0.5$ for several lattice sizes with $L_\tau = 40$. The four (three) leftmost points for $L = 6 (L = 8)$ have been obtained with $\lambda = 0.25$ and $L_\tau = 80, 160, 320, 640$ ($L_\tau = 80, 160, 320$). The continuum line is a fit to $A(T_{\rm c} - T)^{2\beta}$, with $\beta = 0.37$, and $T_{\rm c}$ taken from the $L = 8, 12$ lattices pair (see text).

1. The ferromagnetic Double-Exchange interaction is long-ranged enough to enforce Mean-Field behavior [21]. The critical exponents would be $\nu = 0.5$ and $\eta = 0$.

2. The interaction is not long-ranged enough: the physical behavior should be the one of the classical Heisenberg model in three dimensions [20]. The critical exponents would be $\nu = 0.71(1)$ and $\eta = 0.041(2)$ [22].

In order to decide which of the above possibilities hold, we have applied the quotients-method [23], to the Finite-Size Scaling Ansatz [24]. We recall briefly the basis of this method. Let O be a quantity diverging in the thermodynamical limit as t^{-x_O} ($t = T/T_{\rm c} - 1$ being the reduced temperature). We can write the dependence of O on L and t in the following way [24]

$$O(L,t) = L^{x_O/\nu} \left[F_O \left(\frac{L}{\xi(\infty,t)} \right) + \mathcal{O}(L^{-\omega}, \xi^{-\omega}) \right], \tag{72}$$

where F_O is a (smooth) scaling function and $(-\omega)$ is the corrections-to-scaling exponent (e.g., $-\omega$ is the leading irrelevant exponent of the Renormalization Group transformation). This expression contains the not directly measurable term $\xi(\infty, t)$, but if we have a good definition of the correlation length in a finite box $\xi(L, t)$, Eq. (72) can be transformed into

$$O(L,t) = L^{x_O/\nu} \left[G_O \left(\frac{\xi(L,t)}{L} \right) + \mathcal{O}(L^{-\omega}) \right], \tag{73}$$

where G_O is a smooth function related with F_O and F_ξ and the term $\xi_\infty^{-\omega}$ has been neglected because we are simulating deep in the scaling region. We consider the quotient of measures taken in lattices L and

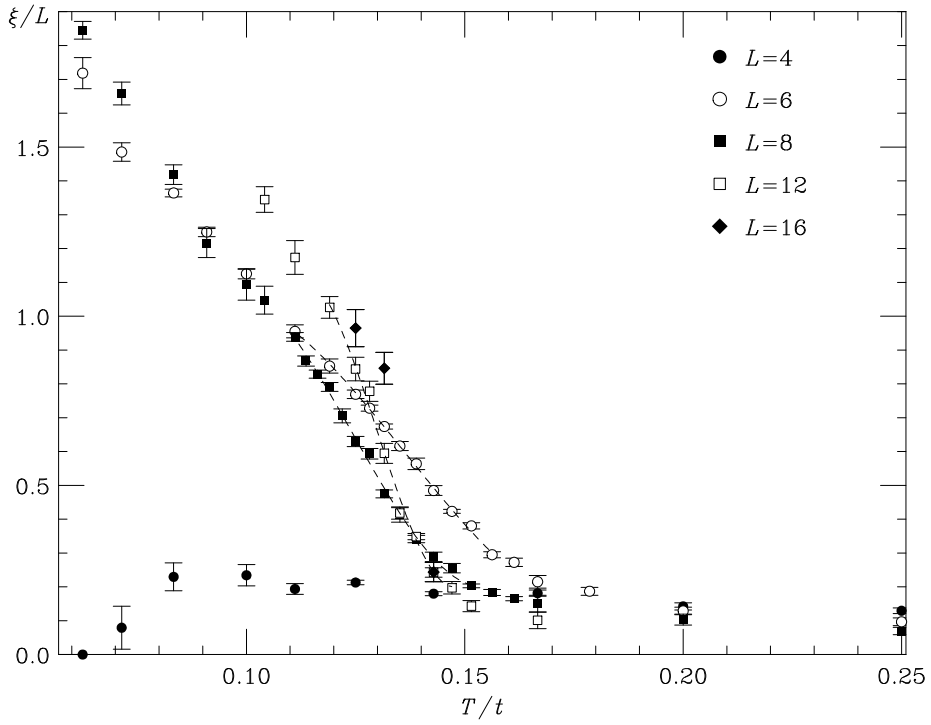


Figure 3: Correlation-length in units of the lattice size as a function of the temperature at $J_{AF} = 0$, $\rho = 0.5$ for several lattice sizes.

sL at the same temperature

$$Q_O(s, L, t) = \frac{O(sL, t)}{O(L, t)}\,. \tag{74}$$

Then, the main formula of the quotient method is

$$Q_O|_{Q_\xi = s} = s^{x_O/\nu} + \mathcal{O}(L^{-\omega})\ , \tag{75}$$

i.e., we compute the reduced temperature t, at which the correlation length verifies $\xi(sL, t)/\xi(L, t) = s$ and then the quotient between $O(sL, t)$ and $O(L, t)$. In particular, we apply formula (75) to the overlap susceptibility, χ, and the β-derivative of the correlation length $\partial_T \xi$, whose associated exponents are:

$$x_{\partial_T \xi} = 1 + \nu\,, \tag{76}$$

$$x_\chi = (2 - \eta)\nu. \tag{77}$$

Notice that $Q_O|_{Q_\xi = s}$ can be measured with great accuracy because of the large statistical correlation between Q_O and Q_ξ. It is also very important that in order to use Eq. (75) one does not need the infinite-volume extrapolation for the critical temperature.

In practice, what we do, is to perform a cubic polynomial fit to ξ/L as a function of T, on the critical region and use the obtained continuous function on the quotients formula (75). We find

$$\nu_{6,12} = 0.75(4), \qquad T_c = 0.1284(9)t \tag{78}$$

$$\nu_{8,12} = 0.72(9), \qquad T_c = 0.1379(6)t\,. \tag{79}$$

The above results are certainly compatible with the classical Heisenberg model exponent, 0.71(1), and are 2.5 standard deviations away from the Mean-Field result, 0.5. The estimate of the critical temperature, shows a considerable lattice size dependency (it can be shown that the crossing point tends to the critical

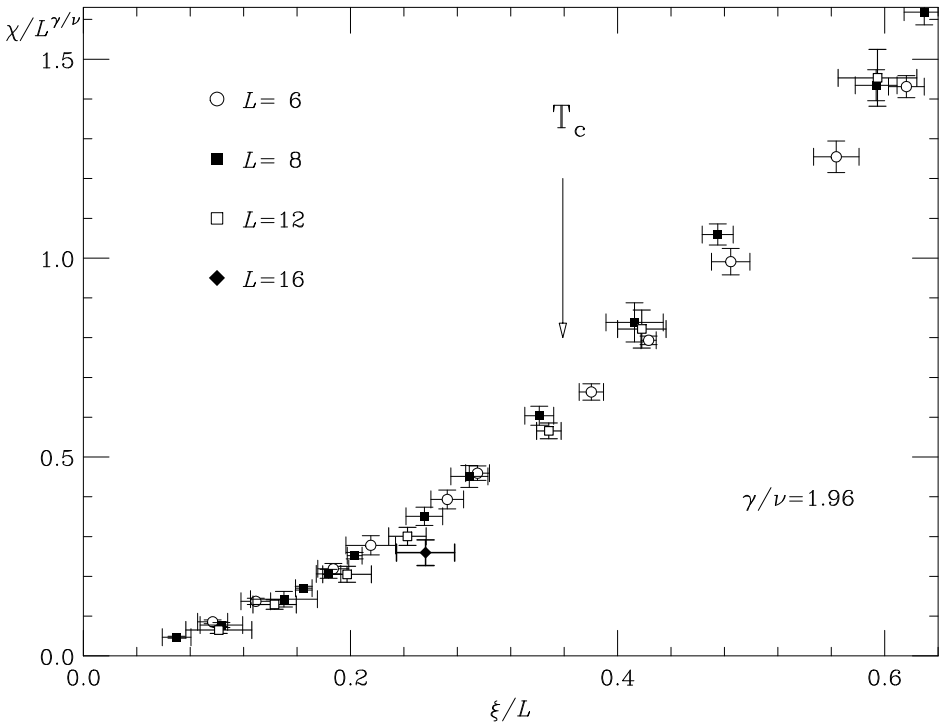


Figure 4: Finite Scaling behavior of $\chi/L^{\gamma/\nu}$, as a function of ξ/L, notice the data collapse. The arrow signals the value of ξ/L at the critical point.

point as $L^{-1/\nu-\omega}$, ω being the universal scaling-corrections critical exponent [23]). Using the crossing point for (8,12) as an estimation of the critical temperature, we can perform a fit of the magnetization squared to the function $A(T_c - T)^{2\beta}$. In Fig. 2 we show a fit with the O(3) exponent $\beta = 0.37$[22] (solid line). The MF value would correspond to a linear behavior ($\beta = 0.5$). It seems therefore safe to conclude that the second scenario is the one realized in Double-Exchange materials with continous transitions, which should have non MF critical beahaviour. Let us however remark that a really accurate measure of critical exponent would require the extension of the reweighting techniques [25] to these models.

It is amusing to observe that the ratio between the real critical temperature at half filling, $T_c \approx 0.14t$, and the variational Mean Field estimate, $T_c^{\rm MF} = 0.19t$ [7], is rather similar to the corresponding ratio for the three dimensional classical Heisenberg model ($T_c = 1.443 J_{\rm AF}$ [22], $T_c^{\rm MF} = 2J_{\rm AF}$).

We finally perform the plot suggested by Eq. (73): $\chi/L^{\gamma/\nu}$ should be an universal function of ξ/L. This seems to be rather well satisfied by our data, with the critical exponents γ and ν of the classical Heisenberg model in three-dimensions.

7 Conclusions and Outlook

We have proposed a general numerical method for studying systems consisting of classical degrees of freedom coupled to fermionic fields. The method is based in the Path Integral formulation of Quantum Mechanics that allows to work in a classical space-time lattice where powerful Monte Carlo techniques, as the Hybrid Monte Carlo method, are applicable since no sign problem arises.

As an example, we have describe explicitly the formulation of the method in the case of the Double Exchange Model, observing that is convenient to use a mapping of the spin to SU(2) matrices to avoid singularities related with the parameterization of the Berry phase.

We have also shown that when the spectrum of the *single-particle* Hamiltonian matrix is bounded, it is possible to work directly in the continuum-time limit, using a *perfect action* thus avoiding the need

for a Trotter-Suzuki extrapolation. We have also shown how to eliminate the spurious dynamical effects induced by the *empty* fermion system, when the spectrum is unbounded.

We have finally presented some numerical results. First we have described some consistency checks and then we have studied a property of the model with direct physical interest as the Paramagnetic–Ferromagnetic transition. We have studied the phase transition at half-filling, where the transition temperature is highest, for simplicity. We have shown that the Finite Size Scaling Ansatz is well satisfied for this model. The critical exponents have turned out to be fully compatible with the ones of the three dimensional classical Heisenberg model, and incompatible with the Mean-Field prediction, as expected on Universality grounds if the interactions are not extremely long-ranged. This conclusion was definitively out of reach with the lattices that could be simulated with previous methods.

Work is in progress for the study of the full phase diagram of the model, $(\rho, T, J_{\rm AF})$. We are also planning to use this Monte Carlo method for the study of models with several electron orbitals and/or phonons.

8 Acknowledgements

We acknowledge financial support from grants PB96-0875, AEN97-1680, AEN97-1693, AEN99-0990 (MEC, Spain) and (07N/0045/98) (C. Madrid). V.M.-M. is a M.E.C. fellow. The simulations have been carried out in RTNN computers at Zaragoza and Madrid.

A Proof of Eqs. (48) and (39)

We recall that $1/T = L_\tau \lambda$ and that the sums (or products) in p_0 run over the Matsubara frequencies (31).

We apply the Poisson summation formula [18] (valid for a continuous (2π)-periodic function)

$$\frac{1}{L_\tau}\sum_{p_0} f(p_0) = \sum_{s=-\infty}^{s=+\infty} (-1)^s \int_{-\pi}^{\pi} \frac{\mathrm{d}t}{2\pi} \mathrm{e}^{\mathrm{i}L_\tau s t} f(t) \tag{80}$$

to the RHS of Eq. (48):

$$\frac{1}{L_\tau}\sum_{p_0} \frac{\mathrm{e}^{\mathrm{i}p_0}}{\mathrm{e}^{\mathrm{i}p_0} - \mathrm{e}^{\lambda(E-\mu)}} = \sum_{s=-\infty}^{s=+\infty} (-1)^s \int_{-\pi}^{\pi} \frac{\mathrm{d}t}{2\pi} \mathrm{e}^{\mathrm{i}L_\tau s t} \frac{\mathrm{e}^{\mathrm{i}t}}{\mathrm{e}^{\mathrm{i}t} - \mathrm{e}^{\lambda(E-\mu)}}\,, \tag{81}$$

$$= \sum_{s=-\infty}^{s=+\infty} (-1)^s \frac{1}{2\pi i} \int_{|z|=1} \mathrm{d}z\ \frac{z^{s\,L_\tau}}{z - \mathrm{e}^{\lambda(E-\mu)}}\,, \tag{82}$$

where the orientation of the contour is positive. For $s < 0$ it is useful to perform the integration in $w = 1/z$.

When $\mu > E$, only the terms $s \geq 0$ contribute, and one obtains

$$\frac{1}{L_\tau}\sum_{p_0} \frac{e^{\mathrm{i}p_0}}{e^{\mathrm{i}p_0} - \mathrm{e}^{\lambda(E-\mu)}} = \sum_{s=0}^{\infty} \left[-\mathrm{e}^{\lambda L_\tau (E-\mu)}\right]^s = \frac{1}{1+\mathrm{e}^{\frac{E-\mu}{T}}}\,, \tag{83}$$

while if $\mu < E$, we need to consider only $s \leq -1$ arriving to

$$\frac{1}{L_\tau}\sum_{p_0} \frac{\mathrm{e}^{\mathrm{i}p_0}}{e^{\mathrm{i}p_0} - \mathrm{e}^{\lambda(E-\mu)}} = -\sum_{s=1}^{\infty} \left[-\mathrm{e}^{-\lambda L_\tau (E-\mu)}\right]^s = \frac{1}{1+\mathrm{e}^{\frac{E-\mu}{T}}}\,. \tag{84}$$

To prove the relation (39), we start noting that (for L_τ even) the products in its LHS can be grouped in pairs of nonzero complex conjugates, so it is possible to write

$$\prod_{p_0} \left(\mathrm{e}^{\mu\lambda + \mathrm{i}p_0} - \mathrm{e}^{\lambda E}\right) = \mathrm{e}^{G(\mu,\lambda,E)} \tag{85}$$

where the function $G(\mu,\lambda,E)$ is real. To obtain G we first compute the μ derivative

$$\frac{\partial G}{\partial \mu} = \sum_{p_0} \frac{\lambda \mathrm{e}^{\mu\lambda + \mathrm{i}p_0}}{\mathrm{e}^{\mu\lambda+ip_0} - \mathrm{e}^{\lambda E}} \tag{86}$$

$$= \lambda L_\tau \frac{1}{1+\mathrm{e}^{\lambda L_\tau (E-\mu)}} \tag{87}$$

$$= \frac{\partial}{\partial \mu} \log\left(1+\mathrm{e}^{-\lambda L_\tau (E-\mu)}\right). \tag{88}$$

From this relation, we know $G(\mu,\lambda,E)$ up to a μ-independent term $G_0(\lambda,E)$

$$G(\mu,\lambda,E) = \log\left(1+\mathrm{e}^{-\lambda L_\tau (E-\mu)}\right) + G_0(\lambda,E)\,. \tag{89}$$

To evaluate G_0 it is enough to observe that

$$\lim_{\mu\to-\infty} \mathrm{e}^{G(\mu,\lambda,E)} = (-1)^{L_\tau} e^{\lambda L_\tau E} \tag{90}$$

$$\lim_{\mu\to-\infty} \log\left(1+\mathrm{e}^{-\lambda L_\tau (E-\mu)}\right) = 0\,, \tag{91}$$

consequently, $G_0 = E/T$ and Eq. (39) follows.

B Integrals over SU(2) and the sphere

In this appendix, we want to show that a generic integral over the sphere

$$\int_{S^2} D\vec{\phi} f(\vec{\phi}) \equiv \frac{1}{4\pi}\int_0^{2\pi} d\varphi \int_0^{\pi} \sin\theta\, d\theta\; f(\theta,\varphi)\,, \tag{92}$$

can be substituted by an integral over the SU(2) group (with Haar's invariant measure).

In order to see how can this be possible, we start noticing that, without loose of generality, the function depending on the vector variable, $f(\vec{\phi})$, can be considered as a function of the matrix $(\vec{\phi}\cdot\vec{\sigma})$, because

$$\phi_i = \frac{1}{2}\mathrm{Tr}\left[\sigma_i(\vec{\phi}\cdot\vec{\sigma})\right] \quad , \quad i=1,2,3\,. \tag{93}$$

Now, one can always find an SU(2) matrix $U[\vec{\phi}]$, such that

$$U[\vec{\phi}](\vec{\phi}\cdot\vec{\sigma})\,U^\dagger[\vec{\phi}] = \sigma_3\,. \tag{94}$$

An explicit choice is given in Eq. (9). There are two important facts to be noticed:

- Two SU(2) matrices, V and W verify $V^\dagger\sigma_3 V = W^\dagger\sigma_3 W$ if, and only if, $V = \mathrm{e}^{\mathrm{i}\alpha\sigma_3}W$ for some α, $-\pi<\alpha<\pi$.
- For any SU(2) matrix, W, there is a point on the sphere $\vec{\phi}_W$, such that $W^\dagger\sigma_3 W = \vec{\phi}_W\cdot\vec{\sigma}$

Therefore, the SU(2) group can be parametrized as

$$W = \mathrm{e}^{\mathrm{i}\alpha\sigma_3}U[\vec{\phi}]\,,\ -\pi<\alpha<\pi\,,\ \vec{\phi}^2=1\,. \tag{95}$$

The above considerations lead us to the following chain of equalities:

$$\int_{S^2} \mathrm{d}\vec{\phi} f(\vec{\phi}) = \int_{S^2} \mathrm{d}\vec{\phi} f(\vec{\phi}\cdot\vec{\sigma}) \tag{96}$$

$$= \int_{S^2} \mathrm{d}\vec{\phi} f\left(U^\dagger[\vec{\phi}]\sigma_3 U[\vec{\phi}]\right) \tag{97}$$

$$= \int_{S^2} \mathrm{d}\vec{\phi}\,\frac{1}{2\pi}\int_{-\pi}^{\pi} d\alpha\; f\left(U^\dagger[\vec{\phi}]\mathrm{e}^{-\mathrm{i}\sigma_3\alpha}\sigma_3\mathrm{e}^{\mathrm{i}\sigma_3\alpha}U[\vec{\phi}]\right) \tag{98}$$

$$= \int_{SU(2)} \mathrm{d}W\, f(W^\dagger\sigma_3 W)\,. \tag{99}$$

So we see that there is at least one integration measure over the SU(2) group, for which our objective can be accomplished. The only thing that still remains to be done is to show that the above integration measure is the proper Haar measure. It will be convenient to recall that the Haar measure is the only one which is right invariant [11], namely for any function F over SU(2), and any SU(2) element V, one should have

$$\int_{SU(2)} \mathrm{d}W\, F(W) = \int_{SU(2)} \mathrm{d}W\, F(WV)\,. \tag{100}$$

But, it is easy to see that if $W = \mathrm{e}^{\mathrm{i}\sigma_3\alpha} U[\vec{\phi}]$, then

$$U[\vec{\phi}]V = \mathrm{e}^{\mathrm{i}\beta(V,\vec{\phi})\sigma_3} U[R_V\vec{\phi}]\,, \tag{101}$$

where R_V is the SO(3) rotation matrix associated with the SU(2) matrix V, in the canonical homomorphism between both groups [12]

$$[R_V\vec{\phi}]\cdot\vec{\sigma} = V^\dagger(\vec{\phi}\cdot\vec{\sigma})V\,. \tag{102}$$

At this point we can just go downhill:

$$\begin{aligned}
\int_{SU(2)} \mathrm{d}W\, F(WV) &= \int_{S^2} \mathrm{d}\vec{\phi}\,\frac{1}{2\pi}\int_{-\pi}^{\pi} d\alpha\; F\left(\mathrm{e}^{\mathrm{i}(\beta(V,\vec{\phi})+\alpha)\sigma_3} U[R_V\vec{\phi}]\right) &(103)\\
&= \int_{S^2} \mathrm{d}\vec{\phi}\,\frac{1}{2\pi}\int_{-\pi}^{\pi} d\alpha\; F\left(\mathrm{e}^{\mathrm{i}\alpha\sigma_3} U[R_V\vec{\phi}]\right) &(104)\\
&= \int_{S^2} \mathrm{d}\vec{\phi}\,\frac{1}{2\pi}\int_{-\pi}^{\pi} d\alpha\; F\left(\mathrm{e}^{\mathrm{i}\alpha\sigma_3} U[\vec{\phi}]\right)\,. &(105)
\end{aligned}$$

In the above expressions, the second equality follows from the periodicity in α of the integrand, while the third is a consequence of the rotational invariance of the measure on the sphere.

In order to formulate the Molecular Dynamics equations of motion, one needs to know how to calculate derivatives on the SU(2) group. For the shake of completeness, we give here the pertinent definitions, but refer to [10] for a complete exposition.

One defines three different derivatives over SU(2) (one per group generator)

$$\partial_j f(U) = \left.\frac{\mathrm{d}\, f(\mathrm{e}^{\mathrm{i}\epsilon\sigma_j}U)}{\mathrm{d}\,\epsilon}\right|_{\epsilon=0}\,. \tag{106}$$

If f is a smooth function of the matrix element of U, $U_{\alpha,\beta}$, we have

$$\partial_j f(U) = \sum_{\alpha,\beta} \frac{\partial f(U)}{\partial U_{\alpha,\beta}}\left(\mathrm{i}\sigma_j U\right)_{\alpha,\beta}\,. \tag{107}$$

If it depends in the full lattice configuration, $\{U_{\boldsymbol{x}}\}$, we define

$$\partial_{\boldsymbol{x},j} f(U) = \sum_{\alpha,\beta} \frac{\partial f(U)}{\partial (U_{\boldsymbol{x}})_{\alpha,\beta}}\left(\mathrm{i}\sigma_j U_{\boldsymbol{x}}\right)_{\alpha,\beta}\,. \tag{108}$$

C The exponential of the single-particle matrix

In this appendix, we show how to numerically deal with the exponential of a matrix, like the Double-Exchange single-particle Hamiltonian matrix, with eigenvalues verifying $-6 \le E_n \le 6$.

Let us call c_n^λ the coefficients of the Legendre polynomials expansion of the function $e^{6\lambda x}$ for $x \in [-1,1]$. We can write

$$\mathrm{e}^{\lambda H_{\mathrm{DEM}}} = \sum_{n=0}^{\infty} c_n^\lambda P_n(H_{\mathrm{DEM}}/6)\,. \tag{109}$$

In the following, we shall use the shortcut $\hat{H} = H_{\rm DEM}/6$. In practice we use the truncation

$$Q(N,\lambda) = \sum_{n=0}^{N} c_n^\lambda P_n(\hat{H})\,, \tag{110}$$

that correspond to a Hamiltonian

$$H^T = \frac{\log Q(N,\lambda)}{\lambda}\,. \tag{111}$$

The truncation error is quantified through the function

$$R_N(x,\lambda) = \frac{\log\left[\sum_{n=0}^{N} c_n^\lambda P_n\left(\frac{x}{6}\right)\right]}{\lambda} - x \quad , \quad x \in [-6,6]\,. \tag{112}$$

that would be zero if the real exponential was calculated. For instance, $R_{10}(x,1/2) < 2\times 10^{-4}$ for all the interval.

To preserve the numerical stability is better to use the recurrence-relations of the Legendre polynomials than their actual expressions in terms of $\hat{H}$. Starting from

$$P_0(\hat{H}) = 1, \quad P_1(\hat{H}) = \hat{H}\,, \tag{113}$$

we will use (for $n > 1$)

$$P_{n+1}(\hat{H})|v\rangle = \frac{2n+1}{n+1}\hat{H}P_n(\hat{H})|v\rangle - \frac{n}{n+1}P_{n-1}(\hat{H})|v\rangle\,. \tag{114}$$

Notice that since matrix $\hat{H}$ is sparse (6 non-vanishing matrix element per row), the truncated expression for the exponential can be calculated in order V operations.

In the HMC, to integrate the equations of motion, we need to know the matrix elements

$$\langle G| \sum_{n=0}^{N} c_n^\lambda \frac{\delta P_n(\hat{H})}{\delta U_{\boldsymbol{x}}}\,|F\rangle\,. \tag{115}$$

From (114) we can write a recursive relation for the derivative. However it would mean a recursion (involving $O(V)$ multiplications) for each lattice site. This would make a total of $O(V^2)$ operations.

Fortunately, it is possible to obtain the matrix elements with $O(V)$ operations. To this end we use the double expansion

$$\frac{\delta P_n(\hat{H})}{\delta U_{\boldsymbol{x}}} = \sum_{m_1=0}^{n-1}\sum_{m_2=0}^{n-1-m_1} L^{(n)}_{m_1,m_2}\, P_{m_1}(\hat{H})\frac{\delta \hat{H}}{\delta U_{\boldsymbol{x}}}P_{m_2}(\hat{H})\,. \tag{116}$$

In this equation $L^{(n)}_{m_1,m_2}$ are symmetric in m_1, m_2 and vanish for $m_1 + m_2 \geq n$. They can be obtained from the following relations

- If $m_1 + m_2 \leq n-2$

$$L^{(n+1)}_{m_1,m_2} = \frac{2n+1}{n+1}\left[\frac{m_1}{2m_1-1}L^{(n)}_{m_1-1,m_2} + \frac{m_1+1}{2m_1+3}L^{(n)}_{m_1+1,m_2}\right] - \frac{n}{n+1}L^{(n-1)}_{m_1,m_2}\,, \tag{117}$$

- if $n-1 \leq m_1 + m_2 \leq n$, with $m_1 \neq 0$

$$L^{(n+1)}_{m_1,m_2} = \frac{2n+1}{n+1}\frac{m_1}{2m_1-1}L^{(n)}_{m_1-1,m_2}\,, \tag{118}$$

- Finally

$$L^{(n+1)}_{0,n} = \frac{2n+1}{n+1}\,. \tag{119}$$

In terms of the L coefficients we can write

$$\langle G| \sum_{n=0}^{N} c_n^\lambda \frac{\delta P_n(\hat{H})}{\delta U_{\boldsymbol{x}}}\,|F\rangle = \left(\sum_{m_1=0}^{N-1}\langle G|P_{m_1}(\hat{H})\right)\frac{\delta \hat{H}}{\delta U_{\boldsymbol{x}}}\left(\sum_{n=0}^{N} c_n^\lambda \sum_{m_2=0}^{n-1-m_1} L^{(n)}_{m_1,m_2}\, P_{m_2}(\hat{H})|F\rangle\right)\,. \tag{120}$$

References

[1] E. D. Wollan and W. C. Koehler, *Phys. Rev.* **100**, 545 (1955); D. I. Khomskii and G. Sawatzky, *Solid State Commun.* **102**, 87 (1997); J. M. D. Coe, M. Viret and S. von Molnar, *Adv. in Phys.* **48**, 167 (1999).

[2] C. Zener, *Phys. Rev.* **82**, 403 (1951); P. W. Anderson and H. Hasegawa, *Phys. Rev.* **100**, 675 (1955).

[3] A.J. Millis, B.I. Shraiman and R. Muller, *Phys. Rev. Lett.* **77**, 175 (1996).

[4] M. J. Calderón, J. A. Vergés and L. Brey, *Phys. Rev.* **B59**, 4170 (1999), and references therein.

[5] A. Moreo, M. Mayr, A. Feiguin, S. Yunoki and E. Dagotto, *Phys. Rev. Lett.*, **84**, 5568 (2000), and references therein.

[6] R.T. Scalettar, D.J. Scalapino y R.L. Sugar, *Phys. Rev.* **B34**, 7911 (1986); S. Duane, A.D. Kennedy, B.J. Pendleton y D. Roweth, *Phys. Lett.* **B195**, 216 (1987).

[7] J. L. Alonso, L. A. Fernández, F. Guinea, V. Laliena and V. Martín-Mayor, cond-mat/0003472, and references therein.

[8] M. Uehara, S. Mori, C. H. Chen and S.-W. Cheong, Nature **399**, 560 (1999); J. M. De Teresa, C. Ritter, M. R. Ibarra, P. A. Algarabel, J. L. García-Muñoz, J. Blasco, J. García and C. Marquina, *Phys. Rev.* **B56**, 3317 (1997); J. Fontcuberta, B. Martínez, A. Seffar, S. Piñol, J. L. Garcia-Muñoz and X. Obradors, *Phys. Rev. Lett.* **76**, 1122 (1996); P. Dai, H. Y. Hwang, C. Kloc and S.-W. Cheong, *Phys. Rev. Lett.* **80**, 4012 (1998); J. Mira, J. Rivas, F. Rivadulla, C. Vázquez-Vázquez, and M.A. López-Quintela, *Phys. Rev. B* **60**, 2998 (1999).

[9] J.L. Alonso, Ph. Boucaud, V. Martín-Mayor and A. J. van der Sijs; *Phys. Rev.* **D61**, 034501 (2000).

[10] See e.g. I. Montvay and G.Münster, *Quantum Fields on a Lattice*, Cambridge University press, Cambridge (1994)

[11] See for instance M. Creutz, *Quark and Gluons on a Lattice*, Cambridge University press, Cambridge (1983)

[12] See e.g. T. Inui, Y. Tanabe and Y. Onodera, *Group Theory and Its aplications in Physics*, Springer-Verlag, Berlin Heidelberg (1990).

[13] See e.g. M. Imada, A. Fujimori and Y. Tokura *Rev. Mod. Phys.* **70**, 1040 (1998)

[14] P. Hasenfratz, F. Karsch, *Phys. Lett.*. **B125**, 308 (1983); J.B. Kogut, H. Matsuoka, M. Stone, H.W. Wyld, S. Shenker, J. Shigemitsum D.K. Sinclair, *Nucl. Phys.* **B225**[FS9], 93 (1983).

[15] G. Batrouni *et al.*, *Phys. Rev.* **D32**, 2736 (1986); S. Gottlieb, W. Liu, D. Toussaint y R.L. Sugar, *Phys. Rev.* **D35**, 2531 (1987).

[16] R. Gupta *et al.*, *Phys. Rev.* **D40**, 2072 (1989).

[17] See, e.g., chapter seven in [10].

[18] See, e.g., chapter four in [10].

[19] F. Cooper, B. Freedman and D. Preston, *Nucl. Phys.* **B210**, 210 (1989).

[20] See e.g. G. Parisi, *Statistical Field Theory*, Addison Wesley, New York, (1988).

[21] For recent work on the crossover between non trivial and trivial critical behavior, see E. Luijten, *Phys. Rev.* **E59** (1999) 4997, and references therein.

[22] H. G. Ballesteros, L. A. Fernández, V. Martin-Mayor and A. Muñoz Sudupe, *Phys. Lett.* **B387**, 125 (1996)

[23] H. G. Ballesteros, L. A. Fernández, V. Martin-Mayor and A. Muñoz Sudupe, *Phys. Lett.* **B378**, 207 (1996); Nucl. Phys. **B483**, 707 (1997).

[24] See for instance M.N. Barber in *Phase Transitions and Critical Phenomena*, vol. 8, edited by C. Domb and J.L. Lebowitz (Academic Press, London, 1983).

[25] M. Falcioni, E. Marinari, M. L. Paciello, G. Parisi and B. Taglienti, Phys. Lett. **B108**, 331 (1982); A. M. Ferrenberg and R. H. Swendsen, Phys. Rev. Lett. **61**, 2635 (1988).